

PACS numbers: 52.38.Ph; 52.50.Jm; 52.59.–f
DOI: 10.1070/QE2010v040n09ABEH014306

Investigation of the foreplasma parameters of a laser-plasma diode

Yu.V. Korobkin, A.I. Lebo, I.G. Lebo

Abstract. **The results of computing experiments are presented, which allow estimating the parameters of the laser foreplasma used to initiate a discharge in a laser-plasma diode. The resultant plasma is a material medium which carries a high-power discharge current. This opens a possibility to make a compact source of hard X-ray radiation and fast-ion streams. Proceeding from our numerical simulations we derive similarity relations, which enable determining the fluxes of plasma mass and charge as functions of laser pulse parameters.**

Keywords: *laser-plasma diode, foreplasma, numerical simulations*

1. Introduction

Investigations aimed at developing a compact source of multiply charged ions and hard X-ray radiation on the basis of laser-induced discharges are pursued in several laboratories [1–5].

The objective of our work is to study the parameters of a foreplasma – the plasma produced by irradiating an aluminium target with high-power short laser pulses, and to analyse experimental data by way of numerical simulation techniques, as well as to derive similarity relations that allow calculating the foreplasma parameters (the mass and the number of free charges). Subsequently it will be possible to use the resultant data for calculating the evolution of the two-component (laser and electric-discharge) plasma and the pinching conditions in the cathode jet of a vacuum laser-induced spark discharge.

2. Physicomathematical formulation of the problem

To estimate the parameters of the plasma produced when a metal target is exposed to a laser pulse, we performed calculations to solve the following system of equations in cylindrical coordinates r, z using the two-dimensional Lagrangian Atlant code [6]:

$$\frac{\mathrm{d}\rho}{\mathrm{d}t} = -\rho\nabla\boldsymbol{v}, \tag{1}$$

$$\rho\frac{\mathrm{d}\boldsymbol{v}}{\mathrm{d}t} = -\nabla(Z_\mathrm{i}p_\mathrm{e} + p_\mathrm{i}), \tag{2}$$

$$Z_\mathrm{i}\rho\frac{\mathrm{d}E_\mathrm{e}}{\mathrm{d}t} = -Z_\mathrm{i}p_\mathrm{e}\nabla\boldsymbol{v} + \nabla(Z_\mathrm{e}\nabla T_\mathrm{e}) - Q_\mathrm{ei} - R_\mathrm{rad}(\rho, Z_\mathrm{i}, T_\mathrm{e}) + \nabla\boldsymbol{q}, \tag{3}$$

$$\rho\frac{\mathrm{d}E_\mathrm{i}}{\mathrm{d}t} = -p_\mathrm{i}\nabla\boldsymbol{v} + \nabla(Z_\mathrm{i}\nabla T_\mathrm{i}) + Q_\mathrm{ei}, \tag{4}$$

$$\left(\frac{\boldsymbol{q}}{|\boldsymbol{q}|}, \nabla\right)\boldsymbol{q} = k_\mathrm{ab}(\rho, T_\mathrm{e})\boldsymbol{q}, \tag{5}$$

$$p_\mathrm{e} = p_\mathrm{e}(\rho, T_\mathrm{e}),\ p_\mathrm{i} = p_\mathrm{i}(\rho, T_\mathrm{i}),\ E_\mathrm{e} = E_\mathrm{e}(\rho, T_\mathrm{e}),\quad E_\mathrm{i} = E_\mathrm{i}(\rho, T_\mathrm{i}),\ Q_\mathrm{ei} = Q_0(Z_\mathrm{i}, A)\frac{T_\mathrm{e} - T_\mathrm{i}}{T_\mathrm{e}^{3/2}}\rho^2. \tag{6}$$

Here, ρ is the plasma density; v is the plasma velocity; E_e and E_i are the specific internal electron and ion energies; T_e, T_i, p_e, and p_i are the electron and ion temperatures and pressures; Q_ei is the term which describes the electron–ion energy exchange rate; Q_0 is the dimensional coefficient which generally depends on the plasma composition; Z_i and A are the ion charge and atomic mass; $\boldsymbol{q}$ is the laser radiation intensity; Z_e and Z_i are the electron and ion thermal conductivity coefficients; k_ab is the radiation absorption coefficient (in the general case it may be defined in tabular form); E_e, p_e pertain to the average charge in a Lagrangian cell; and $R_\mathrm{rad} = R_\mathrm{rad}(\rho, Z_\mathrm{i}, T_\mathrm{e})$ is the plasma energy loss by radiation. The code provides for the inclusion of radiation losses as a function of the above parameters or as a table. In the simplest case of volume losses by bremsstrahlung, this term is of the form $R_\mathrm{rad} = R_0 Z_\mathrm{i}^3\rho^2\sqrt{T_\mathrm{e}}$ and is included only when the plasma is transparent for the bremsstrahlung (R_0 is a dimensional coefficient)*. The physicomathematical model and the methods of solving the above equations are discussed at greater length in a monograph by Lebo and Tishkin [6].

To solve Eqns (1)–(6), use is made of the finite difference method [7] involving splitting in physical processes at every time step. The gas dynamic equations (1), (2) are solved using explicit difference schemes, while the heat transfer equations

Yu.V. Korobkin, A.I. Lebo Moscow State Institute of Radio Engineering, Electronics, and Automation (Technical University), prosp. Vernadskogo 78, 119454 Moscow, Russia;
e-mail: lebo_a_i@mail.ru;
I.G. Lebo Moscow State Institute of Radio Engineering, Electronics, and Automation (Technical University), prosp. Vernadskogo 78, 119454 Moscow, Russia; Scientific Research Institute of System Development, Russian Academy of Sciences, Nakhimovskii prosp. 36, 119991 Moscow, Russia

Received 11 March 2010; revision received 15 April 2010
Kvantovaya Elektronika **40** (9) 811–816 (2010)
Translated by E.N. Ragozin

* In the case of an optically dense plasma, the Atlant code provides for the possibility of performing radiation gas dynamics simulations in a three-temperature approximation (for more details, see Lebo and Tishkin [6]). In the present work this model was not employed.

(3), (4) are solved employing implicit schemes, the transfer coefficients being taken from the previous time step.

The propagation of laser radiation through the plasma is calculated under geometrical optics approximation [Eqn (5)]. The laser beam is represented as a set of discrete rays (ray tracing), the energy being released along the beam path in accordance with the inverse bremsstrahlung mechanism. This approach was first applied to the calculation of laser targets by Friedland and Bernstein [8]; as applied to the Atlant code package, it was first realised by Iskakov et al. [9]. It was assumed in the calculations that laser rays propagated strictly along the z axis.

Three models of the state of matter are incorporated in the code: the model of an ideal gas without inclusion of ionisation and recombination kinetics (the nuclear charge is taken to be the same in all Lagrangian cells); the ZRI model (Zel'dovich–Raizer model with the inclusion of ionisation), and the QEOS (quotidian equations of state) model [10], whereby the thermodynamic plasma parameters are prescribed by way of interpolation of tabulated values. The main ideas for the ZRI model were borrowed from Ref. [11] and described as applied to laser plasmas in Refs [6, 12]. In addition to the equations of state of an ideal two-component (ions and electrons) plasma, elastic terms (p_{ei}) are taken into account for the ion component, according to Ref. [11]:

$$p_i = p_{Ti} + p_{el}, \quad P_{Ti} = n_i T,$$

$$p_{el} = \rho_0 C_s \begin{cases} (\rho/\rho_0)^{\xi} - 1 \text{ for } \rho/\rho_0 \geqslant 1, \\ 0 \text{ for } \rho/\rho_0 < 1, \end{cases}$$

where n_i is the ion density; C_s is the sound velocity in condensed substance; and $\xi = 3-4$.

According to the ZRI model, in each Lagrangian cell the thermodynamic parameters (6) and the ion charge are calculated from the equation for ionisation kinetics

$$\frac{dZ_i}{dt} = Z_i[\varphi_1(\rho, T_e, Z_i) - \varphi_2(\rho, T_e, Z_i) - \varphi_3(\rho, T_e, Z_i)], \qquad (7)$$

where φ_1, φ_2 and φ_3 are the ionisation and recombination rates borrowed from Refs [11, 12]. In this model, Eqn (7) is solved explicitly. In the average ion charge approximation, the energy losses due to ionisation are included by summing the ionisation potential in a Lagrangian cell.

The models were specified above in the order of increasing processor time consumption in the solution of specific problems. It was determined earlier [13] that the radiation–aluminium target interaction simulations performed using the ZRI and QEOS models of the state of matter yielded close results in the $10^{13}-10^{14}$-W cm^{-2} laser intensity range. Below we show that the difference is also small at intensities of $\sim 10^{12}$ W cm^{-2}, and therefore our calculations were primarily performed using the ZRI model.

The expected parameters of Nd-laser radiation are as follows: a pulse energy of 10–100 mJ, a pulse duration of 10–100 ps.

3. Results of numerical simulations

Figure 1 shows the results of two-dimensional simulations of the plasma produced by exposing a 5-μm thick foil to Nd-laser radiation with a wavelength $\lambda = 1.06$ μm and a pulse energy $E_{las} = 50$ mJ. The laser pulse possessed the temporal shape of an isosceles triangle with a base length of 54 ps, the intensity distribution over the beam cross section was $I(r) = \text{const}/\exp(r/R_f)^2$, where $R_f = 160$ μm.

As Fig.1 suggests, in a low-density expanding plasma the maximum charge amounts to 11, the plasma velocity exceeds 300 km s^{-1}, and the ion charge is hardly lowered in the course of expansion (there occurs 'ion charge freezing' [11]). Let us calculate the average charge in the expanding plasma (i.e. in the plasma with a positive velocity component v_z and a density of less than 1 g cm^{-3}) using the formula

$$\overline{Z}_i = \sum_k \Delta M_k Z_{ik} / \sum_k \Delta M_k,$$

where k is the summation index and ΔM_k is the mass of the kth Lagrangian cell. We obtain $\overline{Z}_i \approx 7$. For the most part, the Lagrangian cells with this charge have a density of $10^{-2}-10^{-1}$ g cm^{-3} and an expansion velocity $v_z = 10-200$ km s^{-1}. As this plasma expands, it will partly recombine and, as suggested by two-dimensional simulations, the transverse velocity component v_r increases faster than the longitudinal component v_z.

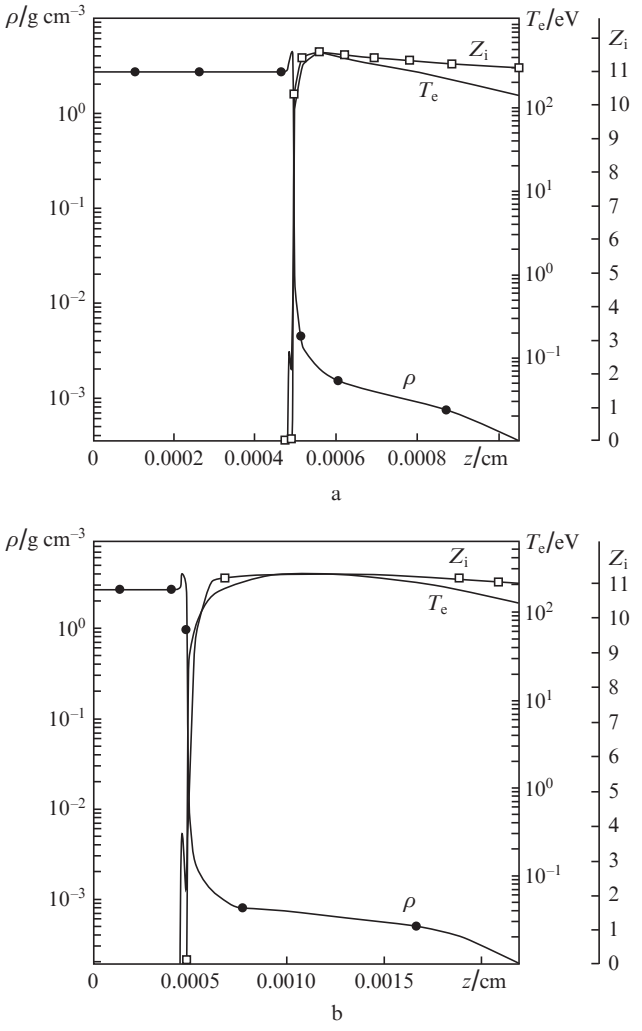

Figure 1. Distributions of the density ρ, the electron temperature T_e, and the charge in the cell Z_i along the z axis for $r = 0$ at the points in time $t = 0$ (a) and 60 ps (b) after the onset of the laser pulse.

Therefore, by the end of the laser pulse the plasma with an ion charge $Z_i \approx 11$ has a density $\rho \leq 10^{-3}$ g cm^{-3} and expands with velocities $300 \leq v_z \leq 3000$ km s^{-1}, the velocity of particle expansion being directed primarily along the z axis (i.e. $v_z \gg |v_r|$). The bulk of plasma mass flies with substantially lower velocities and partly recombines in the course of expansion. The flow directivity pattern of this plasma is much broader than for the plasma with $Z_i \approx 10-11$.

Figure 2 shows the field of electron temperature in the plasma at the point in time $t = 54$ ps (i.e. by the end of the laser pulse). As the radius r increases, the temperature, the expansion velocity, and the ion charge exhibit a slow decrease.

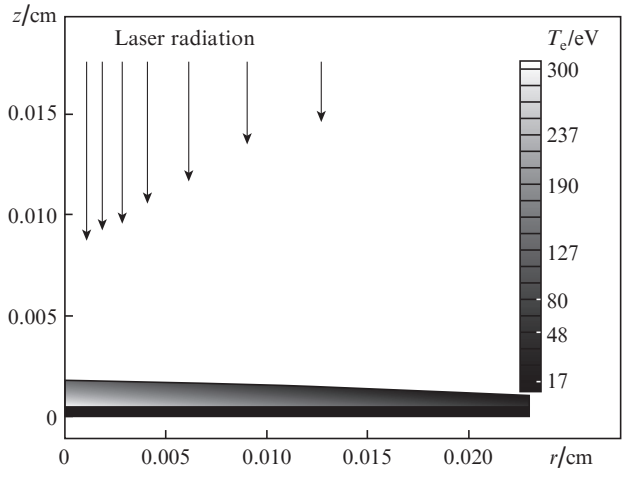

Figure 2. The field of electron plasma temperature at the point in time $t = 54$ s.

One can see from Figs 1 and 2 that that by the end of the laser pulse the longitudinal plasma dimension L_z is substantially shorter than the transverse plasma dimension, namely $L_z \ll R_f$. To the first approximation, the effect of boundary conditions on the plasma flow may therefore be neglected.

In the subsequent simulations we assumed that the intensity of the beam incident on the target is constant in the transverse direction and that the conditions of a perfectly elastic, heat-insulated wall are realised at the right boundary. Therefore, the problem becomes one dimensional and depends only on the variables z and t.

In our calculations we varied the peak intensity I_m of laser radiation, the laser pulse duration τ, and the radiation wavelength λ. We fixed the temporal pulse shape (a right-angled triangle with a base τ and a height I_m) and the target material – a 5-μm thick aluminium foil. Calculations were made of the mass of expanding plasma and the total charge of its ions (and, accordingly, the charge of free electrons, because the plasma is quasi-neutral) as functions of the parameters I_m, τ, and λ.

In the first series of simulations we fixed the pulse duration ($\tau = 30$ ps) and the wavelength of laser radiation ($\lambda = 1.06$ μm), while the intensity I_m was varied. The mass ΔM and charge Z_Q of expanding plasma by the point in time $t = 30$ ps, which were calculated employing the ZRI and QEOS models, are presented in Table 1. (From this point on we give the calculated fluxes of mass ΔM and charge Z_Q across a round area of radius 250 μm.) One can see that the data obtained diverge only slightly, which allowed us to subsequently resort to the more economical model from the standpoint of processor time consumption.

Table 1.

$I_m/10^{12}$ W cm^{-2}	Z_Q/μC		ΔM/ng	
	ZRI	QEOS	ZRI	QEOS
0.21225	38	42.6	2.56	3.1
0.849	96.1	97.2	4.87	4.86
3.4	234	233	9.45	8.83
8.49	387	402	11.5	13
84.9	1781	1770	44.1	44.1

Figure 3 shows the calculated data and their approximation curves. Assuming that the corresponding functions of I_m are power-law dependences, we obtained the following dependences: $\Delta M/\tau \propto I_m^{0.37}$, $Z_Q/\tau \propto I_m^{0.6}$.

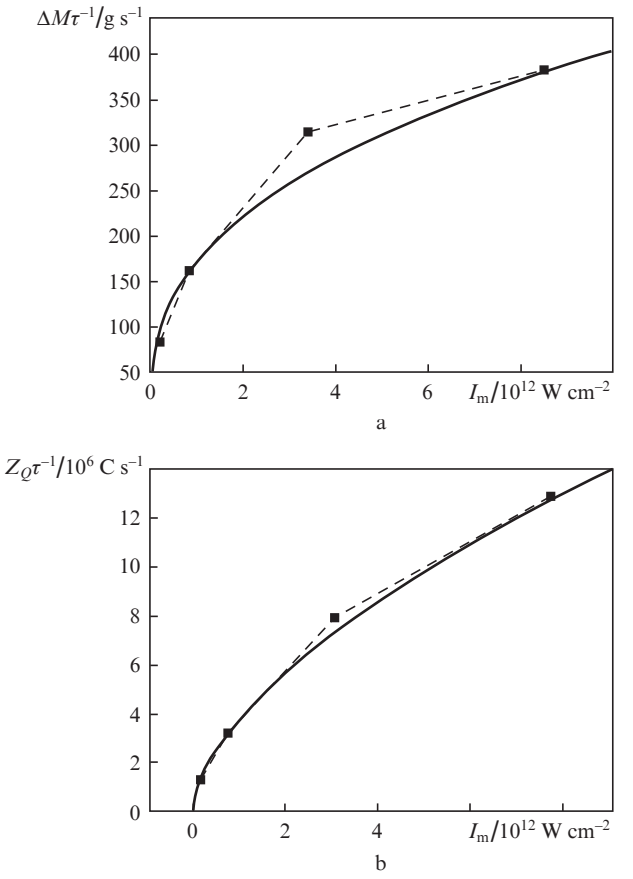

Figure 3. Mass (a) and free charge (b) fluxes in the plasma at the instant of cessation of the laser pulse as functions of radiation intensity I_m. The solid curves are approximations.

In the second series of calculations we fixed the parameters $I_m = 8.49\times10^{11}$ W cm^{-2} and $\lambda = 1.06$ μm, while the pulse duration τ was varied. As a result, we arrived at the following approximative dependences: $\Delta M/\tau \propto \tau^{-0.5}$ and $Z_Q/\tau \propto \tau^{-0.2}$ (Fig. 4).

In the third series of simulations, we fixed the parameters $I_m = 8.49\times10^{11}$ W cm^{-2} and $\tau = 30$ ps and varied the radiation wavelength λ. We obtained the following approximative dependences: $\Delta M/\tau \propto \lambda^{-0.2}$ and $Z_Q/\tau \propto \lambda^{-0.06}$ (Fig. 5).

In all our simulations we assumed that the laser radiation propagated strictly along the z axis and was absorbed in the

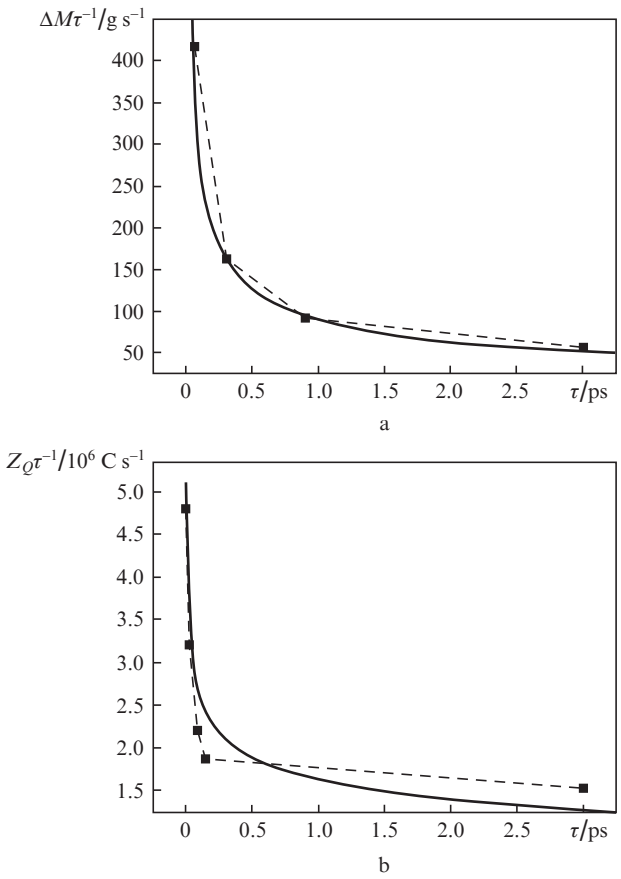

Figure 4. Mass (a) and free charge (b) fluxes as functions of the laser pulse duration. The solid curves are approximations.

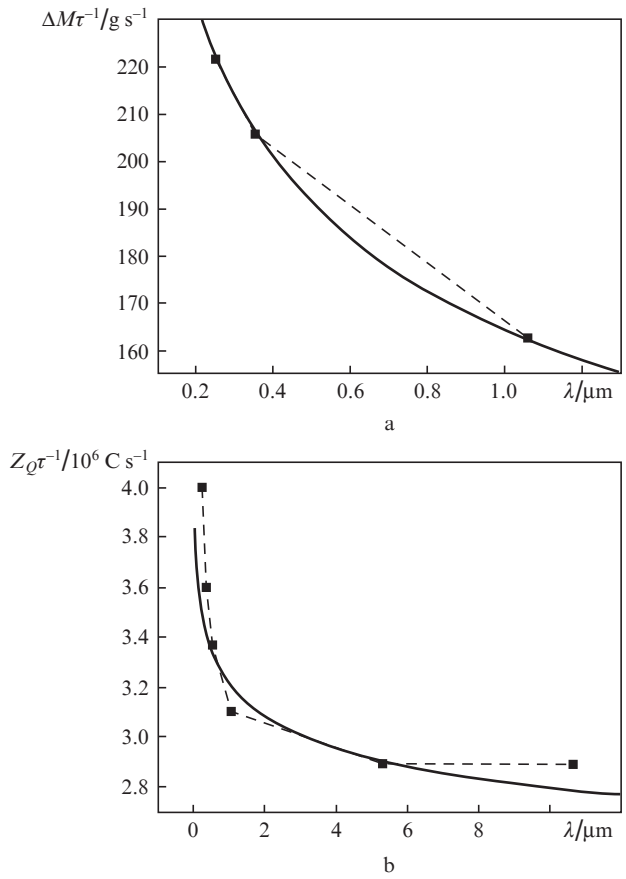

Figure 5. Mass (a) and free charge (b) fluxes as functions of laser radiation wavelength. The solid curves are approximations.

plasma due to the inverse bremsstrahlung mechanism, and that the radiation which reached the critical surface was absorbed in the nearest Lagrangian cell. Therefore, these simulations implied 100% radiation absorption.

Proceeding from the approximations of numerical solutions we obtained the dependences of plasma mass ($\Delta M/\tau$) and charge (Z_Q/τ) fluxes on the parameters specified above (the so-called scaling). Assuming 100% radiation absorption, they are of the form

$$\frac{\Delta M}{\tau} = 8.27\times10^4\left(\frac{I_\mathrm{m}}{I_0}\right)^{0.37}\left(\frac{\tau}{\tau_0}\right)^{-0.5}\left(\frac{\lambda}{\lambda_0}\right)^{-0.2}, \tag{8}$$

$$\frac{Z_Q}{\tau} = 1.63\times10^9\left(\frac{I_\mathrm{m}}{I_0}\right)^{0.6}\left(\frac{\tau}{\tau_0}\right)^{-0.2}\left(\frac{\lambda}{\lambda_0}\right)^{-0.06}, \tag{9}$$

where $\Delta M/\tau$ is taken in g s^{-1} and Z_Q/τ in C s^{-1}. For the basic parameters we selected the following ones: $I_0 = 8.49\times10^{11}$ W cm^{-2}, τ_0 = 30 ps, and λ_0 = 1.06 μm.

On the face of it, the resultant weak dependence of the plasma parameters on the wavelength of laser radiation seems to be strange, since it is known from experiments that the laser-plasma interaction efficiency rises significantly with shortening wavelength. Indeed, shortening the radiation wavelength is attended primarily with an increase of the absorbed fraction of laser energy.

In a one-dimensional formulation of the problem it is possible to employ two models of laser radiation absorption. The radiation propagates strictly along the axis and experiences absorption due to the inverse bremsstrahlung mechanism, and then either reaches the critical surface to be absorbed in its vicinity or is reflected from this surface and follows the corresponding path in the opposite direction (to be partly absorbed due to the inverse bremsstrahlung mechanism). The radiation which reaches the outer plasma boundary is reflected. Relations (8), (9) derived in the foregoing correspond to the first model (100% absorption). The inclusion of strictly backward reflection leads to the dependences of absorbed energy on the duration of laser pulses and the wavelength, which are plotted in Figs 6 and 7. The absorbed fraction of laser energy was calculated by the formula $\eta = (E_\mathrm{las} - E_\mathrm{ref})/E_\mathrm{las}$, where E_las is the incident laser energy and E_ref is the reflected one.

In the fourth series of simulations we fixed the radiation intensity ($I_0 = 8.49\times10^{11}$ W cm^{-2}) and wavelength (λ_0 = 1.06 μm), but changed the pulse duration. One can see from Fig. 6 that the absorbed fraction of laser energy becomes larger with increasing pulse duration, because the plasma corona itself becomes longer. However, this dependence is nonlinear, and the growth rate lowers as the pulse duration increases (as does the energy of the incident laser radiation). We did not succeed in selecting the same power-law dependence of the absorbed energy fraction on the pulse duration for all cases involved. We therefore considered two subdomains: $\tau \geq \tau_0$ and $\tau < \tau_0$, where τ_0 = 30 ps.

In the fifth series of simulations we fixed the duration of the laser pulse (τ_0 = 30 ps) and the radiation intensity ($I_0 = 8.49\times10^{11}$ W cm^{-2}), and varied the radiation wavelength λ. The data of these simulations are given in Fig. 7. One can see that the absorbed energy fraction increases with shortening the wavelength of laser radiation. For the basic laser

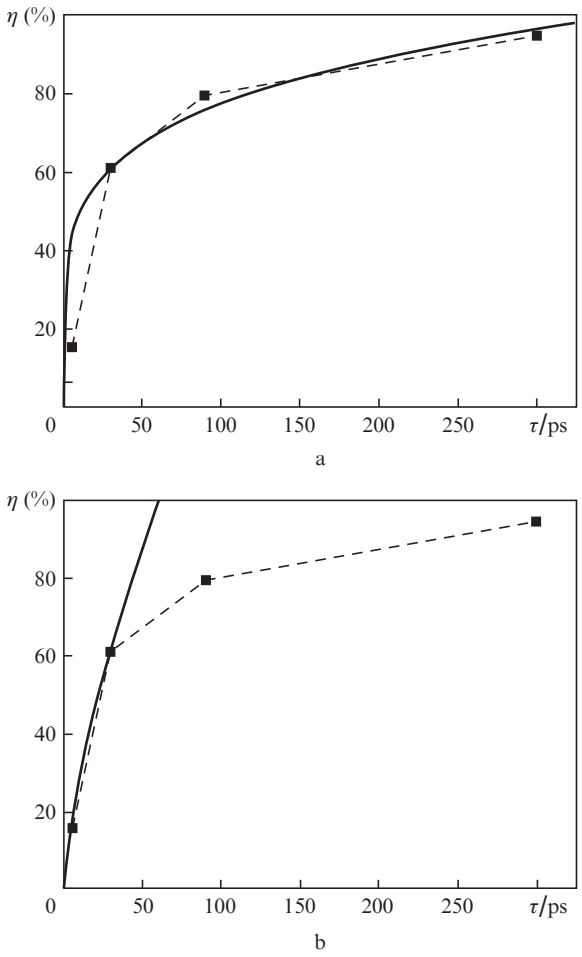

Figure 6. Absorbed fraction η of laser energy as a function of pulse duration for growth exponents $\beta = 0.2$ ($\tau > \tau_0$) (a) and 0.7 ($\tau \le \tau_0$) (b). The solid curves are approximations.

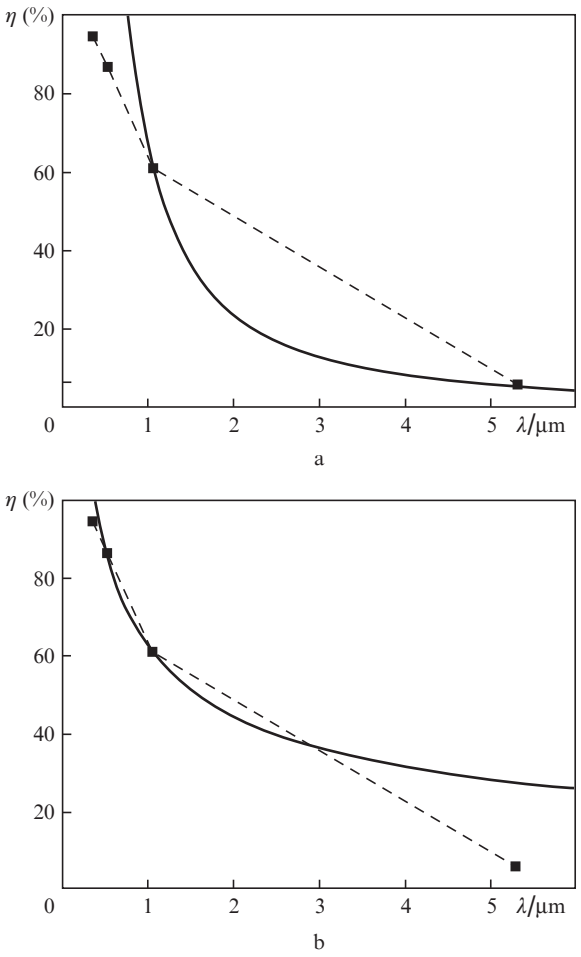

Figure 7. Absorbed fraction η of laser energy as a function of laser radiation wavelength for an exponent $\alpha = -1.5$ ($\lambda > \lambda_0$) (a) and –0.5 ($\lambda \le \lambda_0$) (b). The solid curves are approximations.

parameters ($I_0 = 8.49\times10^{11}$ W cm^{-2}, $\tau_0 = 30$ ps, $\lambda_0 = 1.06$ μm), approximately 60% of the energy is absorbed in the plasma. In the general case, the dependence of absorbed energy fraction on τ and λ is of the form

$$\eta = 0.6\left(\frac{\lambda}{\lambda_0}\right)^{\alpha}\left(\frac{\tau}{\tau_0}\right)^{\beta},$$

$$\alpha = \begin{cases} -0.5, \lambda \leqslant 1\,\mu\text{m}, \\ -1.5, \lambda > 1\,\mu\text{m}, \end{cases} \quad \beta = \begin{cases} 0.7, \tau \leqslant 30\text{ ps}, \\ 0.2, \lambda > 30\text{ ps}. \end{cases}$$

4. Comparison of simulation data with available experimental data

Romanov et al. [5] performed an experimental investigation of some parameters of laser foreplasmas. They obtained the ion charge composition spectra of laser plasmas for three on-target radiation intensities: 5×10^{11}, 4.2×10^{12} and 2×10^{13} W cm^{-2}. The ion energies were shown to amount to 7 keV/Z_i for a target irradiation intensity of 4.2×10^{12} W cm^{-2}. An analysis of the ion charge composition spectra of aluminium produced for different ion energy-to-charge ratios revealed that the highest charge of the ions emitted by the laser plasmas was equal to 5+ and 11+ for target irradiation intensities of 5×10^{11} and 2×10^{13} W cm^{-2}, respectively.

It is pertinent to note, proceeding from experimental conditions, the length of the drift tube in Ref. [5] was equal to 40 cm, and therefore the measured average ion charge was somewhat lower ($\overline{Z}_i \approx 5$) than that calculated for the instant of cessation of the laser pulse ($\overline{Z}_i \approx 7$).

These experimental data are not at variance with the data of numerical simulations given in our work, which testifies to the legitimacy of the assumptions and methods employed in the solution of plasma hydrodynamic equations.

5. Conclusions

The following results were obtained by numerical simulation techniques in our work:

– when an aluminium foil is irradiated by ~100-mJ Nd-laser pulses for an intensity of ~10^{12} W cm^{-2}, there forms a multiply charged ion plasma, which may contain two ion groups: ions with a charge of 10–11, which expand with a velocity of ~500–1000 km s^{-1} (i.e. with an energy of 35–140 keV) and show a preferred expansion direction (perpendicular to the target surface), and the bulk of ions with a charge $Z_i < 7$, which possess an energy of 5–10 keV and a wider directivity pattern;

– we determined the dependence of the plasma mass and free charge fluxes on the intensity, the pulse duration, and the wavelength of heating laser radiation;

– it was confirmed that the fraction of energy absorbed in the plasma increased significantly with shortening the wavelength of laser radiation, and a dependence describing this fact was derived;

– for the conditions considered in our work, the absorbed energy fraction was shown to increase with pulse duration, but its growth rate lowered with lengthening the pulse duration.

Acknowledgements. This work was supported by the Departmental Goal-Oriented Programme 'Development of the Scientific Potential of Higher School (2009–2010)' (Project No. 2.1.1/473) and the Russian Foundation for Basic Research (Grant No. 09-08-01114).

References

1. Korobkin Yu.V., Rozanov V.B., Vergunova G.A., Shikanov A.S. *J. Rus. Laser Res.*, **19** (3), 101 (1998).
2. Korobkin Yu.V., Romanov I.V., Rupasov A.A., et al. *J. Appl. Phys.*, **97** (4), 044303 (2005).
3. Korobkin Yu.V., Paperniy V.A., Romanov I.V., Rupasov A.A., Shikanov A.S. *Plasma Phys. Control. Fusion*, **50**, 1 (2008).
4. Korobkin Yu.V. *Proc. Conf. IRNANO-2009* (Delhi, 2009) p.145.
5. Romanov I.V., Brantov V.A., Paperny V.L., et al. *J. Phys. D: Appl. Phys.*, **43** (3), 035201 (2010).
6. Lebo I.G., Tishkin V.F. *Issledovanie gidrodinamicheskoi neustoichivosti v zadachakh lazernogo termoyadernogo sinteza* (Investigation of Hydrodynamic Instability in Laser Thermonuclear Fusion Problems) (Moscow: Fizmatlit, 2006).
7. Samarskii A.A., Popov Yu.P. *Raznostnye metody resheniya zadach gazovoi dinamiki* (Difference Methods for Solving Problems of Gas Dynamics) (Moscow: Nauka, 1980).
8. Friedland L., Bernstein I.B. *Phys. Rev. A*, **21** (2), 666 (1980).
9. Iskakov A.B., Lebo I.G., Popov I.P., Rozanov V.B., Tishkin V.F. *Kratkie Soobshch. Fiz.*, (1–2), 28 (1997).
10. More R.M. et al. *Phys. Fluids*, **31** (10), 3059 (1988).
11. Zel'dovich Ya.B., Raizer Yu.P. *Physics of Shock Waves and High-Temperature Hydrodynamic Phenomena* (New York: Academic Press, 1966, 1967).
12. Afanas'ev Yu.V., Gamalii E.G., Rozanov V.B. *Trudy FIAN*, **134**, 10 (1982).
13. Lebo A.I., Lebo I.G., Batani D. *Kvantovaya Electron.*, **39** (8), 747 (2008) [*Quantum Electron.*, **39** (8), 747 (2008)].